Huber, A.; Wischmeier, M.; Wiesen, S.; Bernert, M.; Chankin, A. V.; Aleiferis, S.; Brezinsek, S.; Huber, V.; Sergienko, G.; Giroud, C.; Groth, M.; Jachmich, S.; Linsmeier, Ch; Lomanowski, B.; Lowry, C.; Matthews, G. F.; Meigs, A. G.; Mertens, Ph; Silburn, S.; Telesca, G.

The radiated power limit in impurity seeded JET-ILW plasmas

Published in:
Nuclear Materials and Energy

DOI:
10.1016/j.nme.2022.101299

Published: 01/10/2022

Document Version
Publisher's PDF, also known as Version of record

Nuclear Materials and Energy 33 (2022) 101299

Contents lists available at ScienceDirect

Nuclear Materials and Energy

journal homepage: www.elsevier.com/locate/nme

The radiated power limit in impurity seeded JET-ILW plasmas

A. Huber [a,*], M. Wischmeier [b], S. Wiesen [a], M. Bernert [b], A.V. Chankin [b], S. Aleiferis [c], S. Brezinsek [a], V. Huber [d], G. Sergienko [a], C. Giroud [e], M. Groth [f], S. Jachmich [g], Ch. Linsmeier [a], B. Lomanowski [h], C. Lowry [e], G.F. Matthews [e], A.G. Meigs [e], Ph. Mertens [a], S. Silburn [e], G. Telesca [i]

[a] Forschungszentrum Jülich GmbH, Institut für Energie- und Klimaforschung - Plasmaphysik, 52425 Jülich, Germany
[b] Max-Planck-Institut für Plasmaphysik, Boltzmannstraße, 2, D-85748 Garching, Germany
[c] NCSR 'Demokritos', 153 10, Agia Paraskevi Attikis, Greece
[d] Forschungszentrum Jülich GmbH, Supercomputing Centre, 52425 Jülich, Germany
[e] CCFE, Culham Science Centre, Abingdon OX14 3DB, UK
[f] Aalto University, Association EURATOM-Tekes, P.O. Box 4100, 02015 Espoo, Finland
[g] Laboratory for Plasma Physics, ERM/KMS, B-1000 Brussels, Belgium
[h] Oak Ridge National Laboratory, Oak Ridge, TN 37831, USA
[i] Institute of Plasma Physics and Laser Microfusion, Warsaw, Poland

ARTICLE INFO

Keywords:
Impurity
Impurity seeding
High radiation plasma scenarios
JET-ILW

ABSTRACT

The total radiated fraction is examined in high density H-mode plasmas (Greenwald fraction of about 85 %) in JET by the variation of the auxiliary heating power of P_{heat} = 14 MW-29 MW. An achieved radiation fraction of about 75 % at most has been observed in JET-ILW, which is less than the highest achievable (≈90 %) fraction in JET-C during the high radiative power scenarios with N_2 seeding. It is shown that the maximal achievable total radiation fraction averaged over ELM cycles has a strong dependence on the radiation efficiency of the ELM energy, θ_{rad}: $\gamma^{max}_{rad,total} = 1 - \frac{f_{ELM} \times \Delta W_{ELM}}{P_{heat}}(1 - \theta_{rad})$. About 50 % and 16 % of the ELM induced diamagnetic energy drop (ΔW_{ELM}) radiates during the ELM in JET-C and JET-ILW, respectively, which corresponds to the maximum total radiated powers of $\gamma^{max}_{rad,JET-C} = 0.87$ and $\gamma^{max}_{rad,JET-ILW} = 0.77$. These values of the maximum of the radiative power fractions are in good agreement with γ^{max}_{rad} experimentally observed in JET-C (90 %) and JET-ILW (75 %).

1. Introduction

For the safe operation of fusion devices with a burning plasma such as ITER and DEMO, the development of high-radiation plasma scenarios with impurity seeding is necessary to comply with the tight constraints imposed by the material limits of the divertor target plates [1]. To avoid divertor damage, the perpendicular divertor target loads on these machines should be kept below 5 − 10 MWm^{-2} [2,3] (the so-called power density threshold). The observance of this damaging threshold implies a high fraction of radiation: 60–75 % of the total loss power of 150 MW in ITER and 95 % of the loss power in DEMO [1]. Therefore, it is very important to understand the underlying physical processes in highly radiative discharges to establish the radiation limiting mechanism in impurity seeded scenarios.

In this work, dedicated high-radiation seeded experiments were performed with injection of N_2, Ne and Ar as well as with their mixture on JET-ILW tokamak, equipped with the ITER-like wall (ILW: beryllium as first wall and tungsten as divertor armour material). The aim of these experiments was the investigation of the influence of impurity radiations on the plasma confinement, in the plasma core and at the pedestal, of the poloidal radiation distribution and of the recipes for achieving a high radiation fraction, which is the ratio of radiated power to the total heating power, $\gamma_{rad,total} = P_{rad}/P_{heat}$.

In this work we focus on the investigation of mechanisms that limit the maximum radiation. The results achieved during JET campaigns with the ITER-like wall were compared with experiments in the Carbon wall configuration (JET-C) which were operated under similar experimental conditions.

* Corresponding author.
E-mail address: a.huber@fz-juelich.de (A. Huber).

https://doi.org/10.1016/j.nme.2022.101299
Received 30 June 2022; Received in revised form 30 October 2022; Accepted 7 November 2022
Available online 8 November 2022

2. Maximum radiated power in highly radiative H-mode plasma scenarios

2.1. Experiments

At JET-ILW tokamak, equipped with the ITER-like wall (ILW), highly radiative seeded scenarios have been studied with different seeded impurities (N_2, Ne, Ar and their mixture).

The primary goal in these experiments was to investigate how different mixtures affect the radiation patterns, radiation distributions and confinement in the divertor and in the plasma core. It was found [4] that the scenarios with high N_2 seeding rate and correspondingly with high radiation fractions (beyond $\gamma_{rad,total} = 55$ %) are accompanied by moderate confinement degradation, which in turn can be avoided by applying combined impurity seeding. The enhancement of the plasma performance for the radiation fractions beyond $\gamma_{rad,total} = 55$ % was reached with combined N_2 + Ne and N_2 + Ar impurity injections.

Fig. 1 shows the time traces of the plasma parameters in a typical plasma discharge with a combined gas seeding of N_2 and Ne. It shows the line-integrated core and edge electron density measured by interferometry, T_e in the plasma core measured by the ECE diagnostic, the auxiliary NBI and ICRH heating powers as well as the total radiated power, the diamagnetic stored energy, D_2-fuelling and N_2– and Ne-seeding waveforms and the Be II fast emission signal in the inner divertor. The total radiated power, P_{rad}, was measured with help of the metallic resistance bolometer system [5]. It was assessed from the accurate tomographic reconstructions (based on the anisotropic diffusion model [6]) and includes both core and scrape-off-layer (SOL) radiation.

NBI and ICRH heating powers were 18 MW and 4.0 MW respectively to maintain the plasma stored energy (W_{dia}) of 5.0 MJ. N_2 and Ne are injected at the horizontal tiles into the private flux region (PFR): injection rates of 3.6×10^{22}el/s and 2.7×10^{21}el/s for N_2 and Ne respectively. The injection with N_2 is started during the ramp-up phase of the discharge in order to avoid the high heat loads on the divertor and to prevent significant tungsten sputtering and its accumulation during this ramp-up phase. The injection of the mixture N_2 + Ne leads to an increase of the radiation fraction to about$\gamma_{rad,total} = 60$ % ($Z_{eff}\approx 2$) and the normalized confinement following the ITER physics base scaling is around $H_{98(y,2)}\approx 0.77$.

Fig. 2 shows a summary of the reached total radiated fraction during the variation of the auxiliary heating power. A highest achieved radiation fraction of about 75 % has been observed in JET-ILW. In this

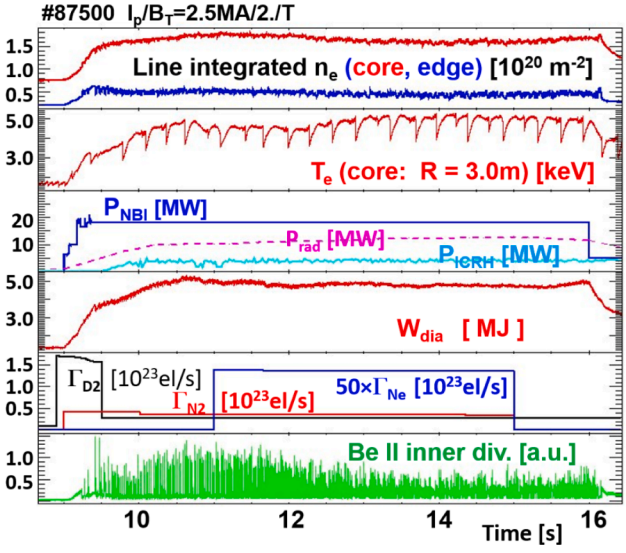

Fig. 1. Time traces of combined N_2 + Ne seeded ELMy H-mode discharge in JET-ILW (#87500).

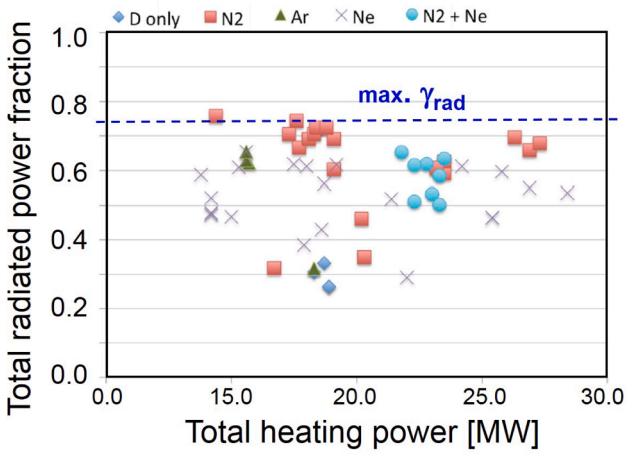

Fig. 2. The total radiation fraction achieved in H-mode plasmas at different heating power inputs.

analysis, the discharges (I_P/B_T = 2.5MA/2.7 T) are performed in a vertical target divertor geometry at the low triangularity configuration ($\delta_{av}\approx 0.25$) in high density H- mode plasmas (Greenwald fraction of about 80–85 %).

In contrast to the JET-ILW, the nitrogen impurity seeded pulses in JET-C with a carbon divertor demonstrate higher radiative power fractions of ≈90 % [7]. In this publication, two questions should thus be clarified:

Why is the radiation in the JET-ILW lower than in JET-C? In addition, it should be explained which maximum power can be radiated.

Before we begin to clarify these questions, it should be noted that replacing the first wall and divertor walls with metallic materials significantly reduced the carbon levels [8], resulting in reduced radiation and Z_{eff}. Under cold detached divertor conditions with significant reduction of W sputtering, the tungsten is introduced into the plasma only during the ELMs. Beryllium is a much weaker radiator than carbon. A comparison between JET-C and JET-ILW plasmas [9] of two plasmas with similar starting parameters (at similar average electron density, and similar input power) shows that the radiative power is reduced in JET-ILW by 1/3 in comparison with JET-C: the radiation fraction $\gamma_{rad,total}$ dropped from 0.45 to 0.3. At the same time, the plasma is cleaner in JET-ILW with the effective charge Z_{eff} reduced from 1.7 to 1.3 owing to the main impurity being now Be instead of C [9].

2.2. Power influx to the SOL

In this section we introduce the power entering the SOL, P_{SOL}, needed for the determination of the maximal achievable total radiation fraction during the inter- and intra-ELM phases. The power flowing through the last closed magnetic flux surface to the scrape-off layer, $P_{SOL,}$ is defined as

$$P_{SOL} = P_{loss} - P_{rad,core} = P_{heat} - P_{rad,core} - dW/dt, \quad (1)$$

where P_{heat} denotes the total heating power given by the sum of the Ohmic power, the neutral beam power and ion cyclotron heating power (where applicable), $P_{loss} = P_{heat} - dW/dt$ the loss power, $P_{rad,core}$ the total radiated power inside the separatrix (core and mantle radiation) and dW/dt the rate of change of the total energy content of the plasma. Core and mantle radiation is caused by line-radiation as well as bremsstrahlung:

$$P_{rad,core} = P_{line} + P_{brems}. \quad (2)$$

Here should be noted, that the radiative power leads to a reduction of the divertor heat fluxes in two stages: firstly, due to the radiation cooling ($P_{rad,core}$) within the separatrix (core and mantle radiation); secondly,

due to the radiation cooling in the SOL and the divertor ($P_{rad,SOL}$) during the inter-ELM phase as well as during the ELMs itself.

Therefore, a power balance analysis could be separated into two phases:

- The inter-ELM phase where the heating recovers the stored energy. The recovery process depends on the loss power, P_{loss}, P_{SOL} and the radiation inside the separatrix and $P_{rad,core}$.
- The ELM phase where the stored energy is lost by the ELM, ΔW_{ELM}.

Taking into the account these two phases, the Eq. (1) can also be written as:

$$P_{SOL} = P_{SOL,inter-ELM} + P_{SOL,ELM} = P_{heat} - P_{rad,core}, \tag{3}$$

Here, the rate of change of stored energy averaged over many ELM cycles is neglected. The power lost by ELMs, $P_{SOL,ELM}$, is defined by

$$P_{SOL,ELM} = f_{ELM} \times \Delta W_{ELM}, \tag{4}$$

where f_{ELM} is the ELM frequency. The strength of ELMs, ΔW_{ELM} is deduced experimentally from the loss in stored plasma energy during the ELM, ΔW_{dia}. From Eqs (3 and 4) one obtains the power crossing the separatrix during the inter-ELM phase:

$$P_{SOL,inter-ELM} = P_{heat} - P_{rad,core} - f_{ELM} \times \Delta W_{ELM}. \tag{5}$$

Thus, the power flowing into the SOL between the ELMs for the plasma discharges at a fixed total heating power, P_{heat}, depends on both the radiation losses in the plasma core and the power losses during the ELM events.

2.3. Achievable radiation fraction during the inter-ELM phase

In this section, we estimate the achievable radiation fraction γ_{rad} in the SOL during the inter-ELM phase. In addition, it should be clarified whether it is possible to radiate the entire $P_{SOL,inter-ELM}$ or a significant part of this power. It should be noted that a major objective of the experiments with impurity seeding is to radiate a large fraction of the power flowing into the SOL to avoid the divertor target damage. At the same time, the core radiation fraction should be minimised to maintain good core confinement.

Let us consider the simple model for power balance in the SOL:

$$q_{||u} = q_{||t} + q_{loss}, \tag{6}$$

where $q_{||u}$ is the upstream parallel power flux density, $q_{||t}$ is the power flux to the target and q_{loss} is the power loss term, given by:

$$q_{loss} = q_{rad,imp} + q_{rad,h} + q_{CX} + q_{\perp}, \tag{7}$$

where $q_{rad,imp} + q_{rad,h}$ is power losses due to the impurity and hydrogen radiations, q_{CX} is the loss due to charge exchange collisions with neutrals. The last term on the right hand side of Eq. (7) represents the perpendicular power loss due the transport processes (diffusive and turbulent transport) across the magnetic field lines [1].

It should be noted that charge exchange reactions transport energy as well as momentum out of a flux tube. Additionally, viscous stress, recombination and friction can contribute to the volumetric momentum or pressure loss. An extended Two Point Model (2PM) [10] is necessary to account for the volume processes that can transport energy, momentum and particles out of a flux tube. Analogously to paper [11] we will define a momentum loss factor for each flux tube as:

$$f_{mom-loss} = 1 - p_t^{tot}/p_u^{tot}, \tag{8}$$

where p_t^{tot} and p_u^{tot} are total divertor target and upstream plasma pressure defined as:

$$p_{tot} = (T_e + T_i)n_e(1 + M^2), \tag{9}$$

with Mach number (M = $v_{||}$/cs with c_s the sound speed and $v_{||}$ the parallel flow velocity) M = 0 at the upstream end of the flux tube and M = 1 at the divertor target.

The pressure balance could be modified as in [11] to

$$(1 - f_{mom-loss})p_u^{tot} = p_t^{tot} = 4n_t T_t \tag{10}$$

The power density $q_{||t}$ transmitted through the electrostatic sheath at the target plate surface, could be expressed as:

$$q_{||t} = \gamma_{sheath} T_{e,t} \Gamma_{||e,t} + \Gamma_{||e,t} \varepsilon_H^{pot}, \tag{11}$$

where $\gamma_{sheath} = 7.5$ [10] is the sheath heat transmission coefficient, $\Gamma_{||e,t} = n_{e,t} c_s$ is parallel particle flux density and $n_{e,t}$ and $T_{e,t}$ the density and temperature at the divertor target. It is assumed here that $T_i = T_e$ and the plasma is flowing at the isothermal sound speed $c_s = \sqrt{2kT_{e,t}/m_i}$ at the target with Mach number M = 1 (Bohm–Chodura sheath condition [12], where m_i is the fuel ion mass ($m_i = 2 \times m_p = 3.35 \times 10^{-27}$ kg and $m_i = 2.5 \times m_p = 4.18 \times 10^{-27}$ kg for pure deuterium and deuterium–-tritium plasmas, respectively). The last term on the right hand side of the Eq. (11) represents the flux of the potential energy of ions and neutrals due to their degrees of ionisation and dissociation. Impinging ions implanted into the divertor target recombine to neutral atoms and partially diffuse to the target surface. Depending on the surface concentration of hydrogen atoms as well as surface temperature, they can recombine to molecules. The form of the reemission (atomic or molecules) depends strongly on the surface temperature [13]. In this contribution we will use the simple assumption that the potential energy from the recombination processes is $\varepsilon_H^{pot} = 13.6eV + 2.25eV \approx 15.8eV$ which includes the hydrogen ionization energy and half of the molecular binding energy. Finally, it is released as heat and contributes to the deposited power.

In addition to impurity radiation losses, the hydrogenic radiation, $q_{rad,h} = \Gamma_{||e,t} \varepsilon_H^{rad}$, could contribute significantly to the total power losses and should be taken into the account when considering the power and particle fluxes to the divertor. Here, it is assumed that each recycled atom radiates an energy ε_H^{rad} of about 15 eV [14] in the form of line radiation before being ionized. But in general this value depends on the electron temperature as well as on the electron density.

The maximum theoretically achievable radiative fraction, $\gamma_{rad,tot}$ could be calculated assuming that only impurity and hydrogen radiation contribute to the power losses:

$$q_{loss} = q_{rad,imp} + q_{rad,h} = q_{rad,tot}^{SOL} \tag{12}$$

Taking this assumption, the power balance Eq. (6), is now modified to:

$$q_{||u} = \gamma_{sheath} T_{e,t} n_{e,t} c_s + n_{e,t} c_s \varepsilon_H^{pot} + q_{rad,tot}^{SOL}, \tag{13}$$

From power balance (12) and pressure balance (10) equations, the maximum achievable $\gamma_{rad,tot}$ and the impurity radiation fraction $\gamma_{rad,imp}$ are then obtained:

$$\gamma_{rad,tot} = 1 - \frac{c_s}{4}\left(\gamma_{sheath} + \varepsilon_H^{pot}/T_t\right)\left[\frac{p_{u,tot}}{q_{||u}}\right] \times (1 - f_{mom-loss}) \tag{14}$$

$$\gamma_{rad,imp} = 1 - \frac{c_s}{4}\left(\gamma_{sheath} + \left(\varepsilon_H^{pot} + \varepsilon_H^{rad}\right)/T_t\right)\left[\frac{p_{u,tot}}{q_{||u}}\right] \times (1 - f_{mom-loss}) \tag{15}$$

The evaluated Eqs. (14 and 15) are consistent with the achievable power dissipation derived by Stangey and Pitcher [11,14] from the extended 2PM. According to the Eqs (14 and 15), the achievable radiative fraction decreases with upstream pressure and increases with increasing power flux density. Fig. 3 shows the maximum achievable radiative fraction in the SOL of ITER and JET for two cases: 1) case with $f_{mom-loss} = 0$ with constant pressure along field lines, 2) case with $f_{mom-loss} = 0.9$ with a high pressure loss. The maximum impurity radiated power fraction occurs at $T_t^{crit} = \left(\varepsilon_H^{pot} + \varepsilon_H^{rad}\right)/\gamma_{sheath} \approx 4eV$ and is around

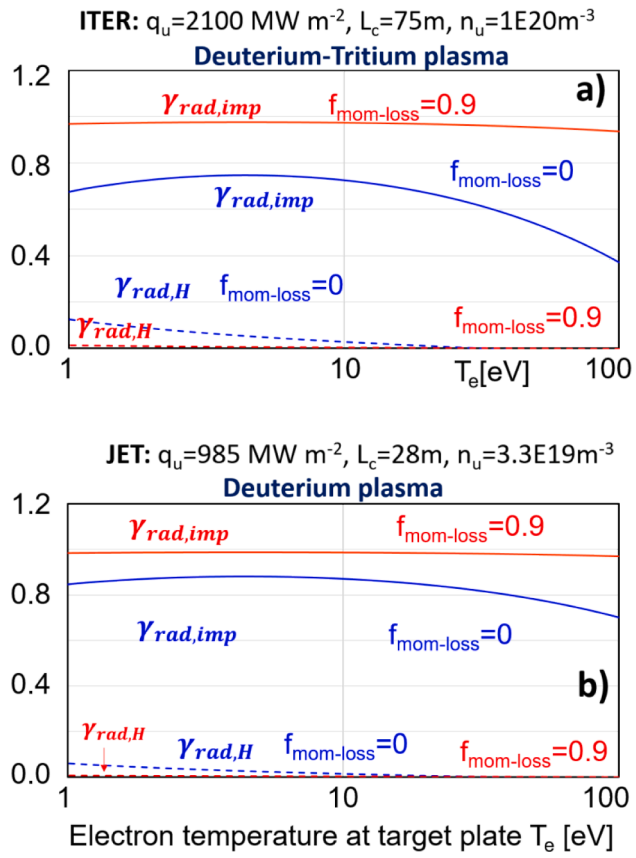

Fig. 3. Impurity and hydrogen radiation fractions as functions of the electron temperature at the divertor target for a) ITER and b) JET-ILW cases.

$\gamma_{rad,imp} = 0.7$ calculated for an example of ITER [14]: $q_{||u} = 2100 MWm^{-2}$, connection length $L_c = 75$ m, $n_u = 10^{20} m^{-3}$. The JET SOL at $q_{||u} = 985 MWm^{-2}$, connection length $L_c = 28$ m, $n_u = 3.3 \times 10^{19} m^{-3}$ demonstrates a $\gamma_{rad,imp} \approx 0.84$.

As is shown in [15,16], the operation at target temperature $T_t < T_t^{crit}$ may lead to unstable or periodically oscillating divertor regimes under the conditions with constant pressure along field lines ($f_{mom\text{-}loss} = 0$). On the other hand for a significant momentum loss ($f_{mom\text{-}loss} \neq 0$) there is no bifurcation and the electron temperature at the target T_t can be reduced to extremely low values by decreasing the $\frac{p_{u,tot}}{q_{||u}}$ ratio to extreme values [10].

When the pressure is conserved, in high recycling regime the impurity radiation is limited. On the other hand, a decrease of divertor temperature under constant pressure conditions leads to an increase in particle fluxes. At the same time, the flux of the potential energy $\Gamma_{||e,t} \varepsilon_H^{pot}$ and hydrogenic radiation $\Gamma_{||e,t} \varepsilon_H^{rad}$ increases too. Fig. 3 shows that in contrast to $f_{mom\text{-}loss} = 0.9$, the high recycling regime ($f_{mom\text{-}loss} = 0$) demonstrates a significant hydrogen radiation at T_e below 3–5 eV. On the other hand, under conditions where the recycle flow is significantly reduced and there is a significant pressure drop across the recycle region, the hydrogen radiation fraction is negligible. In this case, the radiation fraction, which is mainly due to the impurity radiation, can increase to almost 1.0.

2.4. Maximum achievable total radiation fraction: During the intra-ELM phases

The dependence on the ELM energy drop ΔW_{ELM} of the radiated plasma energy which follows the ELM crash has been analysed in JET-C and described in details in [17]. It is reported that the radiated plasma energy is proportional to the ELM energy:

$$P_{rad,ELM} \sim \Delta W_{ELM} = \theta_{rad} \times \Delta W_{ELM} \quad (16)$$

where θ_{rad} is coefficient which is depending the wall material of the machine.

2.5. Maximum achievable total radiation fraction averaged over the inter- and intra-ELM phases

Taking into account the findings from Section 2.3 it is assumed for the calculation of the maximum achievable radiation power that the entire power $P_{SOL,inter\text{-}ELM}$, crossed during the inter-ELM phase is radiated: $P_{rad,\ inter\text{-}ELM} = P_{SOL,inter\text{-}ELM}$.

It follows from the Eq. (5)

$$P_{rad,inter-ELM} = P_{heat} - P_{rad,core} - f_{ELM} \times \Delta W_{ELM} \quad (17)$$

It follows that the maximum of the total radiated power can be written as:

$$P_{rad,total}^{max} = P_{rad,inter-ELM} + P_{rad,core} + P_{rad,ELM} = \quad (18)$$

$$= P_{heat} - f_{ELM} \times \Delta W_{ELM} + \theta \times f_{ELM} \times \Delta W_{ELM}, \quad (19)$$

From Eq. (19) follows the maximum achievable total radiation fraction:

$$\gamma_{rad,total}^{max} = 1 - \frac{f_{ELM} \times \Delta W_{ELM}}{P_{heat}} (1 - \theta_{rad}), \quad (20)$$

3. Discussion

As shown in Eq. (20), the maximum radiated power averaged over the ELM cycles depends strongly on the main ELM parameters, f_{ELM} and ΔW_{ELM}. Also on the efficiency of the radiation during the ELM event, θ_{rad}. With increase of the ELM frequency the ELM energy decreases because the ELM size, ΔW_{ELM}, is inversely proportional to the ELM frequency f_{ELM} [18] ($\Delta W_{ELM} \sim 1/f_{ELM}$) for a given heating power. At the same time, the fraction of ELM transported power, $f_{ELM} \times \Delta W_{ELM}/P_{heat}$, is constant between 20 % and 30 % [19,18] as observed on several fusion machines with carbon divertor such as JET, DIII-D, and ASDEX Upgrade in H-mode plasmas with type I ELMs. This fraction is also constant at the JET-ILW and is about $P_{SOL,ELM}/P_{heat} \approx 0.27$ for the highly radiative H-mode plasmas reported in this contribution. The ratio $P_{SOL,ELM}/P_{heat}$ on the JET-C and JET-ILW is thus nearly similar and cannot explain the differences in the radiation fraction for JET with different wall materials. On the other hand, the fraction of the radiated ELM energy could have a significant impact on the maximum of the total radiated fraction.

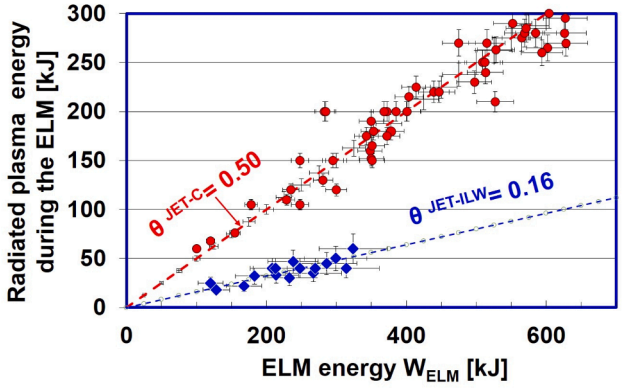

Fig. 4. Radiated plasma energy during the ELM event versus the ELM energy: red symbols JET-C; blue symbols JET-ILW. (For interpretation of the references to colour in this figure legend, the reader is referred to the web version of this article.)

Fig. 4 presents the dependence on the ELM energy drop ΔW_{ELM} of the radiated plasma energy which follows the ELM crash. In this case the radiated energy includes only the radiated losses integrated over the first main peak of the ELM. The algorithm used here in this work is similar to that described in [20]. As is shown in Fig. 4, the radiated plasma energy is proportional to the ELM energy for JET-C and JET-ILW. About 50 % of the ELM energy drop radiates with the ELM in JET with carbon divertor. In contrast to JET-C, the discharges in JET-ILW radiate significant lower fraction of the ELM energy, about 16 %. Note that due to the limited time resolution of the JET bolometer system [5], the radiated plasma energy during the ELM has been evaluated on the time scale of about 2–4 ms what is larger than the ELM duration t_{ELM}, in which the ELM deposits its energy on the target. The distribution of the ELM duration found in JET-C and JET-ILW has been intensively investigated in contribution [21]. In JET-C, the average value of t_{ELM} is about 750 μs with a smaller variance of the ELM duration distribution. In contrast to JET-C, the average ELM duration in JET-ILW is larger (about 2 ms in comparison to 750 μs observed in the JET-C) and the distribution is wider. However, the shortest ELMs in the configuration with ILW achieve the values observed in the JET-C. Due to the short ELM duration, it is unlikely that the radiated energy during the ELM period is significant. On the other side, the ELM could ablate the deposits on the exposed divertor targets, which are known to exist on the inner divertor target [22], resulting in an increased divertor radiation. The ELM-induced carbon release may be due to the thermal decomposition [23] and ablation of deposited layers [22]. The target surface temperature during the transient loads as measured with infra-red thermography reaches peak values significantly below 2000 °C at the inner target. Even the maximum measured value of 2000 °C is too low for bulk carbon ablation, but it is enough to provoke an ablation of the deposited layers in the inner divertor [17,24]. The results of post-mortem analyses of the JET-ILW divertor tiles show that the inner divertor remains the region of highest deposition in the inner divertor [25]. Secondary ion mass spectrometry (SIMS) and ion beam analysis (IBA) measurements in this region show that deposits are beryllium (Be) dominated. Beryllium is a much weaker radiator than carbon. As a result, the JET-ILW radiates significantly lower fraction of the ELM energy during the ELM event (which includes the ELM energy transport to the divertor target as well as the phase when the ablated deposits are radiated), about of ≈1/3 (=16 %/50 %) of the radiated fraction in the JET-C configuration.

For the fraction of ELM transported power, $f_{ELM}\times\Delta W_{ELM}/P_{heat}$, of 0.27 and the radiated fractions $\theta_{rad}^{JET\text{-}C} = 0.5$ and $\theta_{rad}^{JET\text{-}ILW} = 0.16$, the evaluated maximum of the total radiated powers gives $\gamma_{rad,\ JET-ILW}^{max} = 0.77$ and $\gamma_{rad,\ JET-C}^{max} = 0.87$ for the JET with ILW and carbon divertor, respectively. The maximum of the radiative power fractions of ≈90 % has been reached in JET-C which is in good agreement of the estimated value of 0.87. Also, the maximum achieved for the radiation fraction of about 70–75 % in JET-ILW is compatible with the estimated $\gamma_{rad,\ JET-ILW}^{max} = 0.77$. The lower experimental values could be explained by the overestimation of the NBI power. An energy balance analysis based on tile thermocouples for JET-ILW [26] reveals that, typically, 25 % of the nominal energy input was unaccountable when compared to the sum of the all losses. It was reported that an error is co-linear with the neutral beam injection heating. However, a detailed error analysis for the NBI system suggests an error of not more than 10 % in the power calculation whereas a ~ 20 % reduction would be required to match the average energy balance. It should be mentioned that the source of the imbalance is still an open question and further analysis is required. Assuming the overestimation of the NBI heating power by 10 % will bring the experimentally measured maximum achieved radiation fraction to values of 77–83 % which are in quite good agreement with the estimated value of 0.77 for the JET-ILW.

Assuming that the energy flux to the wall in the main chamber is negligible, the ELM energy transported to the divertor targets could be written as $E_{target}^{ELM} = f_{ELM} \times \Delta W_{ELM}\times(1\text{-}\theta) \times \tau$, where τ is the time duration of the ELMy-H mode phases. For a JET pulse with a relatively high input energy of 153 MJ (plasma discharge 87500, with N_2 seeded impurities shown in Fig. 1), the ELM energy coupled to the divertor targets is about $E_{target}^{ELM} = 37$ MJ ($P_{SOL,ELM}$≈5.3 MW). This pulse had 18 MW of NBI power and the 4.0 MW of ICRH power applied for about 7.0 s: $P_{heat} = 23.1$ MW.

The energy absorbed at the divertor tiles is measured by calorimetry [27] which is based on measuring the cool down time evolution of the tiles between pulses. This requires that the time taken for a tile to come to internal thermal equilibrium is short compared to the cooling time due to conduction and Planck radiation. The energy delivered to divertor tiles in the analysed pulse 87500 is about $E_{TC} = 59.6$ MJ. Since the divertor is completely detached in this plasma pulse, the absorbed energy is based on the ELM energy and the energy deposited by the radiation itself: $E_{TC} = E_{ELM} + E_{rad}$.

To calculate the poloidal radiation distribution, hence the radiation load onto the vessel, the tomographic reconstruction model in use has been coupled with a Monte-Carlo technique [28,17]. Calculated with this method, the radiation energy which is supplied to the divertor amounts to about $E_{rad} = 17.9$ MJ. After subtraction of the energy deposited by the radiation, the evaluated ELM deposited energy is $E_{ELM} = 41.7$ MJ which is, under consideration of the accuracy of the calorimetric method, is in agreement with the $E_{target}^{ELM} = 37$ MJ. This agreement confirms the correctness of Eq. (7).

Considering ITER machine, where the expected total radiation fraction mentioned in the introduction of this paper is 60–75 %, and assuming that the fraction of $f_{ELM}\times\Delta W_{ELM}/P_{heat}$ is similar to JET-ILW of ≈0.27, we obtain a θ_{rad} coefficient of about 0.1 for the radiation fraction of $\gamma_{rad,total} = 0.75$. This value for the ITER-like wall material composition is below the JET-ILW value ($\theta_{rad} = 0.16$) and is therefore feasible.

As it was shown above, the radiated ELM energy has a big impact on the total radiated fraction. Besides, a significant part of the $P_{SOL,inter\text{-}ELM}$ could be radiated between the ELMs. Taking these results into account, one way to increase the radiation fraction is to achieve an ELM-free H-mode phase by strongly increasing the injection rate of seeded impurities. Those seeded plasmas were described in [1,17,29]. Fig. 5 shows the time traces of such a H-mode N_2-seeding discharge which has been carried out at JET-ILW. The impurity, in this case the nitrogen gas, was injected into the private flux region of the outer divertor leg with a seeding rate of Γ_{N2}≈13.4 × 10^{22}el/s. The time traces show ELMs with relatively small energy directly after the L-H transition, with a fast transition at 10.8 s from a Type I ELMy to a stable and stationary ELM-free H-mode phase. This phase was previously specified as M−mode [30] with medium plasma performance between H-mode and L-mode.

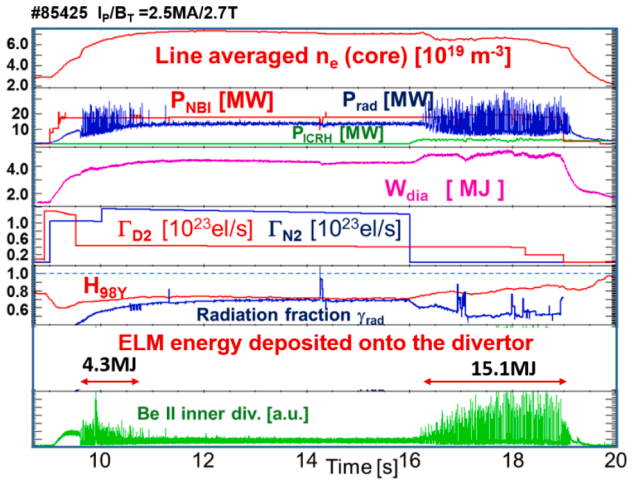

Fig. 5. Time traces of central line averaged n_e, auxiliary heating powers, NBI and ICRH, as well as total radiated power, plasma stored energy, D_2-fuelling and N_2-seeding waveforms, γ_{rad} and $H_{98(y,2)}$-factor, and fast BeII- emission line signal in the inner divertor.

The discharge demonstrates a cold pedestal with the pedestal temperature of $T_{e,ped}\approx 330$ eV during this ELM-free H-mode and energy confinement factor, $H_{98(y,2)}$, of about 0.75. Despite an enormously strong impurity injection rate, the radiation fraction reaches only the value of $\gamma_{rad} \approx 75$ %. The estimated total ELM energy coupled to the divertor targets is about $E_{target}^{ELM} = 19.6$ MJ ($<P_{SOL,ELM}> \approx 5.1$ MW) and is in agreement with the measured $E_{ELM} = 19.6$ MJ: the measured total energy which includes the radiation itself is $E_{TC} = E_{ELM} + E_{rad} = 19.6$ MJ + 28.5 MJ = 48.1 MJ. The total input energy of 191 MJ shows however a strong energy disbalance of about 50 MJ: we find 48.1 MJ in the divertor and 90 MJ radiation loads on the main chamber wall. What is also noticeable is that the absorbed energy of 48.1 MJ in the divertor is too small. This disbalance could be explained by the power losses from the pedestal region due to the charge exchange processes: $D^+ + D^0 \rightarrow D^0 + D^+$. The heat load from hot D^0 neutrals is distributed over the entire first wall area and is not measurable on the JET machine.

Assuming the neutral density around $10^{16} m^{-3}$ in the transport barrier region and assuming a half of the CX power density as loss, we will obtain the following estimation for the power losses [31]

$$P_{CX-loss}/V = 1/2\langle\sigma v\rangle_{CX} n_d n_e 3/2T_i \quad (21)$$

where $<\sigma v>_{CX} \approx \sigma_{CX} \times v$ is the rate coefficient for the CX reactions with $\sigma_{CX} = 2.2 \times 10^{-19}$ m^2 and v = 2×10^5 m/s taken from [32] for $T_i = T_e = 330$ eV. For $n_{ped} = 4.3 \times 10^{19}$ m^3, it gives the following expression for $P_{CX-loss}/V \approx 0.75 MJ/m^3$. Assuming that the localized area, where the CX reactions take place intensely, has a radial extension of about 6 cm, we obtain a volume of about 7.1 m^3 and power losses of about $P_{CX\text{-}loss} = 5.3$ MW. The first wall energy heat load from the CX neutrals could be estimated to 5.3 MW × 9 s ≈48 MJ and can therefore explain the mentioned disbalance of 50 MJ. This power loss is comparable to the $<P_{SOL,ELM}> \approx 5.1$ MW explaining the stability of this ELM-free regime: the radial gradient of the plasma pressure in the transport barrier is stable and below the critical value if $P_{CX-loss} \geq <P_{SOL,ELM}>$, while keeping the total P_{sol} above the L-H power threshold.

It should be noted that charge exchange from neutral deuterium onto impurity ions leads to strong modifications of the ionisation equilibrium of seeded impurities in the pedestal region. CX causes a higher abundance of lower ionised stages and a concomitant increase of the pedestal radiation by impurities [33].

Thus, at the extremely highest radiation level with the cold pedestal, the neutral density rises and could lead to increased CX power losses, thus limiting the radiation fraction.

It should be noted that estimates for neutral power losses are coarse. The aim of this assessment was to bring the point in the discussion and to show that the power losses of the neutrals could theoretically explain the strong energy imbalance in the ELM-free H-mode discharges. The physics of power losses through neutral is very complex and requires detailed edge modelling to fully understand it.

3. Conclusions

Highly radiative conditions with N_2, Ne and Ar as well as their mixture as radiators are approached in JET H-mode plasmas with a fully metallic first wall. Highly radiating JET-ILW H-mode plasmas with enhanced plasma performance (up to $H_{98(y,2)} = 0.78$) for radiation fractions beyond $\gamma_{rad,total} = 55$ % have been achieved with combined N_2 + Ne and N_2 + Ar impurity injections.

The total radiated fraction is examined at high plasma density (Greenwald fraction of about 85 %) by the variation of the auxiliary heating power of $P_{heat} = 14$ MW-29 MW. An achieved radiation fraction of about 75 % at most has been observed. In contrast to the JET-ILW, the nitrogen impurity seeded pulses in JET-C with a carbon divertor demonstrate higher radiative power fractions of ≈90 % [7].

It was shown that the fraction of the radiated ELM energy, θ_{rad}, has a considerable influence on the maximum of the total radiated fraction, $\gamma_{rad,total}^{max} = P_{rad}/P_{heat}$. The evaluated maximum achievable total radiation fraction has the following dependence on the main ELM parameters:

$$\gamma_{rad,total}^{max} = 1 - \frac{f_{ELM} \times \Delta W_{ELM}}{P_{heat}}(1 - \theta_{rad}) \quad (22)$$

In JET with carbon divertor (JET-C), about 50 % of the ELM induced diamagnetic energy drop (ΔW_{ELM}) radiates during the ELM [17]. In contrast to JET-C, the discharges in JET-ILW radiate a significantly lower fraction of about 16 % of ΔW_{ELM}. The different radiated fractions during the ELMs could be explained by ELM-induced ablation of the deposits on the exposed divertor targets, resulting in an increased divertor radiation during the ELM events. In contrast to the Be rich layers in JET-ILW, the JET-C deposit layers contain mainly carbon which radiates much more efficiently than beryllium. It should be mentioned that the footprint of the heat loads on the divertor targets during the inter-ELM phase is typically the erosion area. However, the position of the strike point moves outboard (positive dR) during an ELM [34], to the area of the deposited layers and thus causes an ELM-induced ablation of the deposited layers. The strike point later moves back to the pre-ELM position.

For the fraction of the ELM total power into scrape-off layer, $f_{ELM} \times \Delta W_{ELM}/P_{heat} = 0.27$ (typical values for both JET-ILW and JET-C) and the radiated fractions during the ELMs $\theta_{rad}^{JET\text{-}C} = 0.5$ and $\theta_{rad}^{JET\text{-}ILW} = 0.16$, the estimated maximum of the total radiated powers gives $\gamma_{rad,JET-ILW}^{max} = 0.77$ and $\gamma_{rad,JET-C}^{max} = 0.87$ for the JET with ILW and carbon divertor respectively. These values of the maximum of the radiative power fractions are in good agreement with γ_{rad}^{max} experimentally observed in JET-ILW (75 %) and in JET-C (90 %). Additionally, the estimated ELM energy transported to the divertor targets, E_{target}^{ELM}, is in good agreement with values measured by thermocouples for the ELM deposited energy of E_{ELM}.

For ITER the expected θ_{rad} coefficient is of about 0.1 for $\gamma_{rad,total} = 0.75$. Here, we assume that the fraction of $f_{ELM} \times \Delta W_{ELM}/P_{heat}$ at ITER is similar to JET-ILW and is of ≈0.27.

At the extreme highest radiant level in the free-ELM H-mode regime with the cold pedestal, the neutral density increases and results in increased CX power losses, thereby limiting the radiant fraction.

Note:

JET contributors* See the author list of Overview of JET results for optimising ITER operation by J. Mailloux et al. to be published in Nuclear Fusion Special issue: Overview and Summary Papers from the 28th Fusion Energy Conference (Nice, France, 10–15 May 2021).

Author contribution

A. Huber[a]: main author, experiments, data analysis, analytical calculation.

M. Wischmeier[b] – experiments, analysis.

S. Wiesen[a] - experiments, analysis.

M. Bernert[b]: experiments, analysis.

A.V. Chankin[b]: analytical calculation.

S. Aleiferis[c]: data analysis.

S. Brezinsek[a]: experiments, data analysis,

V. Huber[d]: experiments, data analysis,

G. Sergienko[a]: experiments, data analysis,

C. Giroud[e], M. Groth[f], S. Jachmich[g], Ch. Linsmeier[a], B. Lomanowski[h], C. Lowry[e], G. F. Matthews[e], A. G. Meigs[e], Ph. Mertens[a], S. Silburn[e], G. Telesca[i]: experiments, data analysis,

Declaration of Competing Interest

The authors declare that they have no known competing financial interests or personal relationships that could have appeared to influence the work reported in this paper.

Data availability

Data will be made available on request.

Acknowledgements

This work has been carried out within the framework of the EUROfusion Consortium, funded by the European Union via the Euratom Research and Training Programme (Grant Agreement No 101052200 — EUROfusion). Views and opinions expressed are however those of the author(s) only and do not necessarily reflect those of the European Union or the European Commission. Neither the European Union nor the European Commission can be held responsible for them.

References

[1] M. Wischmeier, et al., J. Nucl. Mater. 463 (2015) 22–29.
[2] A. Loarte, et al., Nucl. Fusion 47 (2007) S203–S263.
[3] A.R. Raffray, et al., Fusion Eng. Des. 85 (2010) 93–108.
[4] A. Huber, et al., Phys. Scr. 2020 (T171) (2020), 014055.
[5] A. Huber, et al., Fusion Engineering and Design 82 (2007) 1327–1334.
[6] L.C. Ingesson, B. Alper, H. Chen, et al., Nucl. Fus. 38 (1998) 1675.
[7] J. Rapp, et al., Nucl. Fusion 44 (2004) 312–319.
[8] S. Brezinsek, et al., J. Nucl. Mater. 438 (2013) S303–S308.
[9] C. Giroud et al., Nucl. Fusion 53 (2013) 113025 (12pp) doi:10.1088/0029-5515/53/11/113025.
[10] P.C. Stangeby, The Plasma Boundary of Magnetic Fusion Devices, Institute of Physics Pub, Bristol; Philadelphia, 2000, p. 232.
[11] P. C. Stangeby et al., Plasma Phys. Control. Fusion 60 (2018) 044022 (38pp).
[12] P.C. Stangeby, Physics of Plasmas 2 (1995) 702, https://doi.org/10.1063/1.871483.
[13] P.h. Mertens, et al., Plasma Phys. Control. Fusion 43 (2001) A349–A373.
[14] C. S. Pitcher and P. C. Stangeby P C, Plasma Phys. Control. Fusion 39 (1997) 779.
[15] S.I. Krasheninnikov, A.S. Kukushkin, A.a. Pshenov, Phys. Plasmas 23 (2016), 055602.
[16] K. Borrass K, Nucl. Fusion 31 (1991)1035.
[17] A. Huber, et al., J. Nucl. Mater. 415 (2011) S821–S827.
[18] A., Herrmann Plasma Phys, Control. Fusion 44 (2002) 883–903. PII: S0741.
[19] A.W. Leonard 1999 J. Nucl. Mater. (1999) 266–269 109.
[20] J.C. Fuchs, T. Eich, A. Hermann, et al., J. Nucl. Mater. 337–339 (2005) 756.
[21] B. Sieglin, et al., Plasma Phys. Control. Fusion 55 (2013), 124039.
[22] J.P. Coad, et al., Nucl. Fusion 46 (2006) 350.
[23] A. Kreter, et al., Phys. Rev. Lett. 102 (2009), 045007.
[24] J. D. Strachan, W. Fundamenski, M. Charlet et al., Nuclear Fusion 43 (2003) 922.
[25] A. Widdowson, et al., Nucl. Mater. Energy 12 (2017) 499–505.
[26] G.F. Matthews, et al., Nuclear Materials and Energy 12 (2017) 227–233.
[27] G.F.Matthews et al., J. Nucl. Mater. 290-293 (2001) 668-672.
[28] A. Huber, et al., Journal of Nuclear Materials 390–391 (2009) 830–834.
[29] A. Huber et al Impact of Strong Impurity Seeding on the Radiation Losses in JET with ITER-like Wall, in: Proc. of the 41th EPS Conference on Controlled Fusion and Plasma Physics, Berlin, 2014), 2014 http://ocs.ciemat.es/EPS2014PAP/pdf/P1.031.pdf , P1.031.
[30] E.R. Solano, et al., Nuclear Fusion 57 (2017), 022021.
[31] R. Dux, private communication.
[32] R.K. Janev, J.J. Smith, Atomic and Plasma Material Interaction Data for Fusion (Atomic and Plasma Material Interaction Data for Fusion no 4), INTERNATIONAL ATOMIC ENERGY AGENCY, Vienna, 1993 https://www.iaea.org/publications/1839/atomic-and-plasma-material-interaction-data-for-fusion.
[33] R. Dux, et al., Nucl. Fusion 60 (2020), 126039.
[34] E.R. Solano, et al., Nucl. Fusion 48 (2008), 065005.